EUROPEAN ORGANIZATION FOR NUCLEAR RESEARCH

CERN–EP/98–105
5 June 1998

STUDY OF CHARGE TRANSPORT IN NON-IRRADIATED AND IRRADIATED SILICON DETECTORS

C. Leroy, P. Roy
Université de Montréal, Montréal (Québec) H3C 3J7, Canada

G. Casse[1], M. Glaser, E. Grigoriev, F. Lemeilleur
CERN, Geneva, Switzerland

ABSTRACT

The electrical characteristics of non-irradiated and irradiated n-type silicon detectors ($p^+ - n - n^+$ diode) are extracted by fitting a charge transport model to a set of experimental data obtained from the measurement of the current pulse response induced by α and β particles. The detectors were irradiated with either ≈ 1 MeV neutrons up to a fluence of 9.92×10^{13} n/cm^2 or with 24 GeV/c protons up to a fluence of 10.6×10^{13} p/cm^2. After n- to p-type inversion, a small junction on the p^+ side of the detector is introduced to fit the experimental data and to account for the evolution of the electrical characteristics of the detectors with fluence.

Presented at the 2nd International Conference on Radiation Effects on Semiconductor Materials, Detectors and Devices, Florence, 4–6 March 1998

[1] Associazione per lo Sviluppo Scientifico e Technologico del Piemonte (ASP)

1 INTRODUCTION

The movement of the charge carriers generated by an ionizing particle in a detector produces a signal the shape of which is determined by the charge transport properties of the detector. A standard $p^+ - n - n^+$ diode is considered. Three main parameters are likely to change when a detector is damaged: the effective concentration of dopants (N_{eff}) which defines the internal electric field and thus the depletion voltage, the electron (μ_e) and hole (μ_h) mobilities which influence the time needed to collect the charge, and the charge trapping lifetime (τ_{th}, τ_{te}) which affects the efficiency of the charge collection. Silicon diodes were irradiated with either ≈ 1 MeV neutrons at the CERN PSAIF up to a fluence $\Phi = 9.92 \times 10^{13}$ n/cm^2 or with 24 GeV/c protons at the CERN PS up to a fluence $\Phi = 10.6 \times 10^{13}$ p/cm^2 in order to investigate the possible changes with fluence of the properties of the silicon devices that will be used in the future high-energy physics experiments at CERN's Large Hadron Collider.

We present a model which describes the transport of the charge deposited by α and β particles in non-irradiated and irradiated silicon detectors. The model is used to fit the experimental signal-current pulse response induced by α and β particles. From these results, the silicon detector electrical characteristics such as N_{eff}, μ_e, μ_h, τ_{te} and τ_{th} can be extracted.

2 CHARGE TRANSPORT MODEL

A planar semiconductor ($p^+ - n - n^+$ diode) is considered, with the ohmic side and the junction side located at $x = 0$ and $x = w$, respectively. Assuming a single trap state, the transport of carriers is described by the Poisson and current continuity equations:

$$\begin{aligned} \nabla^2\psi &= -\nabla E = -\frac{q}{\varepsilon}(-N_{\text{eff}} - n + p - n_t + p_t) \\ \frac{\partial c}{\partial t} &= -\frac{\partial c_t}{\partial t} \pm \frac{\nabla J}{q} + g - Rc - U_{SRH} \\ \frac{\partial c_t}{\partial t} &= \frac{c}{\tau_{tc}} - \frac{c_t}{\tau_{dc}} - Rc_t \ , \end{aligned} \tag{1}$$

where ψ, E and g are the electrostatic potential, the electrical field, and the electron-hole pair generation terms, respectively. The density of the free and trapped carriers (n for electrons or p for holes) are c and c_t, respectively. All these variables are a function of position and time. The minus sign (of the $\pm$) is used for the holes, $N_{\text{eff}} = N_a - N_d$ is the effective concentration of dopants (N_d for n-type, N_a for p-type), q the electric charge, ε the permittivity, and τ_t and τ_d the trapping and detrapping lifetime. The first equation takes into account a plasma effect when the electron and hole densities are of the order of the effective concentration of dopants. The carriers are thus shielding themselves from the external electric field and take a longer time to be collected.

The current density of the carriers is given by:

$$J = qc\mu_c E \pm \mu_c k_{\text{B}} T \nabla c \ , \tag{2}$$

where μ_c (μ_e or μ_h) is the field-dependent mobility, k_{B} the Boltzman constant and T the temperature.

The Shockley–Read–Hall generation-recombination term is given by:

$$U_{\text{SRH}} = \frac{np - n_i^2}{(p + n_i)\tau_{th} + (n + n_i)\tau_{te}} \ , \tag{3}$$

where n_i is the intrinsic carrier density. A term of transverse outflow R [1] in the last two equations takes the transverse diffusion into account:

$$R = \frac{18D_a}{18D_a t + r_0^2} \ , \tag{4}$$

where D_a is the ambipolar diffusion constant and r_0 the initial radius of the column of charges.

The boundary and initial conditions on the densities of the carriers are given by:

$$c(0,t) = c(w,t) = c_t(x,0) = 0 \quad \text{and} \quad c(x,0) = g(x) \ . \tag{5}$$

When neglecting the size of the p^+ and n^+ regions, the integration of Poisson's one-dimensional equation at $t = 0$, for a simple abrupt pn junction operated in the overdepleted mode ($V_b > V_d$), gives (Fig. 1):

$$E(x,0) = -\frac{qN_{\mathrm{eff}}}{\epsilon}x + \frac{V_b}{w} + \frac{V_d N_{\mathrm{eff}}}{w|N_{\mathrm{eff}}|} \qquad \text{for } 0 < x < w \tag{6}$$

$$E(0,t) = E(w,t) = 0 \tag{7}$$

$$\psi(0,t) = V_0 + \psi_p \approx 0 \qquad \text{and} \qquad \psi(w,t) = \psi_p - V_b \approx -V_b \ , \tag{8}$$

where $V_0 \approx 0.6$ V is the built-in voltage, V_b the applied bias voltage, $\psi_p \approx -0.3$ V the electrostatic potential of the neutral p-type region, and V_d is the full depletion bias voltage.

The generation function, g in Eq. (1) at time $t = 0$ is given by:

$$g(x) = \frac{n_0 \times \mathrm{density}(x)\delta(x - x_0)}{\sum_{x'} \mathrm{density}(x')} \qquad \text{with } x_{\mathrm{min}} \leq x_0 \leq x_{\mathrm{max}} \ . \tag{9}$$

For an α particle of 5.0 MeV in silicon ($\approx$ 0.5 MeV is lost in air), the number of electron-hole pairs created is $n_0 \approx 1.4$ million pairs over a range $r = x_{\mathrm{max}} - x_{\mathrm{min}} \approx$ 25 μm, whilst the density of the electron-hole pairs is obtained by an interpolation between the data of Ref. [2] shown in Fig. 2. For a β particle in silicon, the range exceeds the physical size of the detector and a uniform density of electron-hole pairs is created with $n_0 \approx 80$ pairs/μm.

For electric field values around 10^4 V/cm, the drift velocity of the charge carrier reaches the saturation value v_{sc} ($v_{sh} = 10^7$ cm/s and $v_{se} = 1.05 \times 10^7$ cm/s for holes and electrons, respectively). The resulting value for the mobility as a function of the electric field is:

$$\mu(x) = \frac{\mu_{c0}}{[1 + (\mu_{c0}E(x)/v_{sc})^m]^{1/m}} \ , \tag{10}$$

where μ_{c0} is the zero field mobility, $m = 1$ for the holes and $m = 2$ for the electrons.

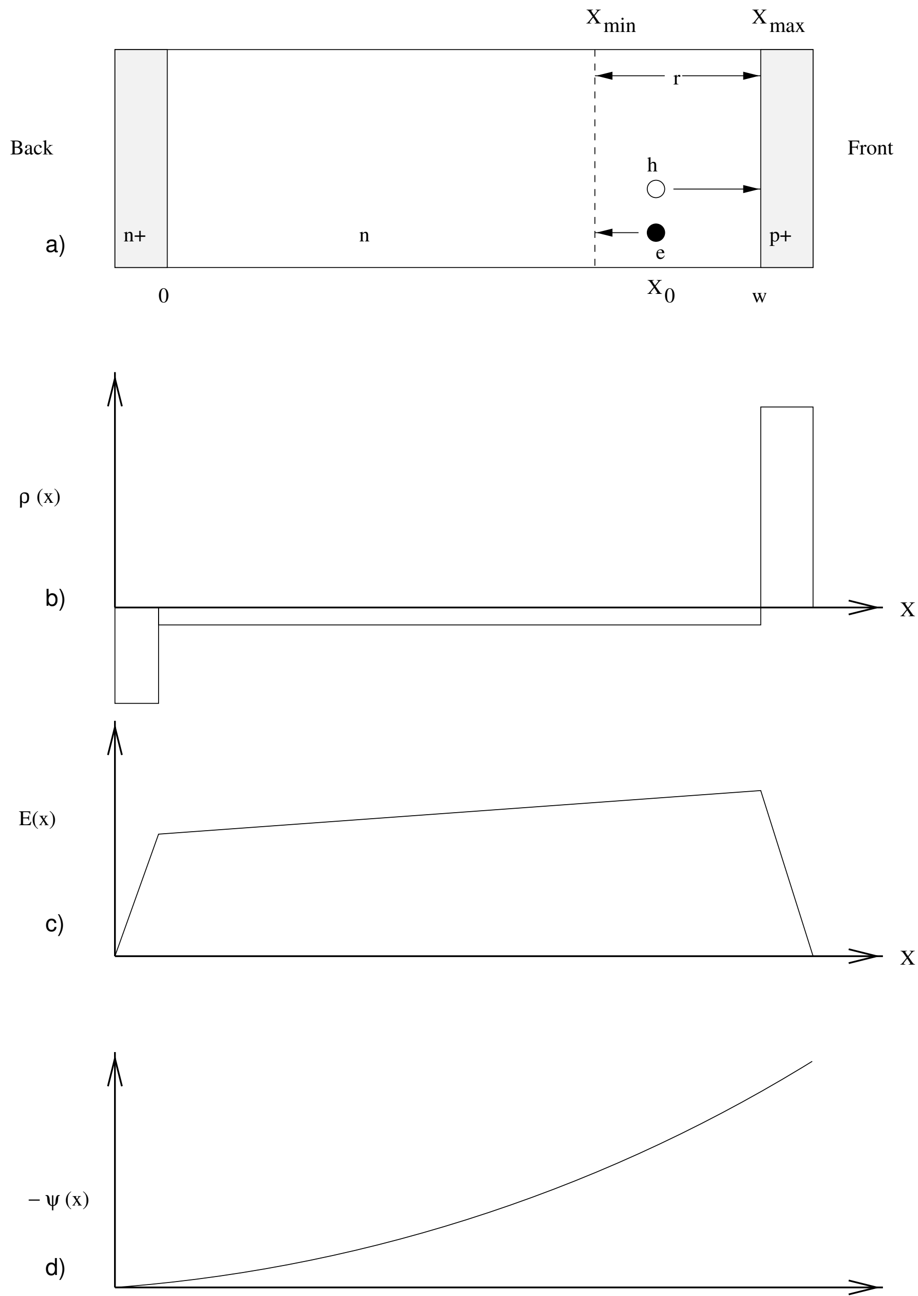

Figure 1: a) Representation of a $p^+ - n - n^+$ diode, b) its dopant profile (ρ), c) its electric field (E), and d) its electrostatic potential (ψ)

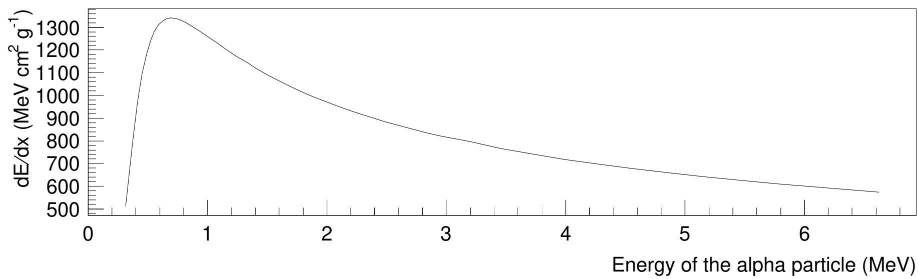

Figure 2: Energy deposit of an alpha particle in silicon

The mobilities are also dependent on the temperature and on the doping concentration [3]. The effect of the concentration is only appreciable for concentrations over 10^{14} dopants/cm^3, and therefore has no influence in the present work. However, every change of temperature by 1.5°C changes both mobilities by $\approx$ 1%. These features are taken into account through:

$$\mu(T, N_{\rm eff}) = \mu_{\rm min} + \frac{\mu_0 \left(\frac{T}{300}\right)^{\nu} - \mu_{\rm min}}{1 + \left(\frac{T}{300}\right)^{\xi} \left(\frac{N_{\rm eff}}{N_{\rm ref}}\right)^{\alpha}} \,, \quad (11)$$

where $\mu_{\rm min} = 55.24$ and 49.7 for the electron and the hole, respectively; $N_{\rm ref} = 1.072 \times 10^{17}$ and 1.606×10^{17} for the electron and the hole, respectively; $\nu = -2.3$ and -2.2 for the electron and the hole, respectively; $\xi = -3.8$ and -3.7 for the electron and the hole, respectively; $\alpha = 0.73$ and 0.70 for the electron and the hole, respectively. In this work, Eq. (11) is used at room temperature.

3 EXPERIMENTAL SET-UP

Electrons from a ^{106}Ru source with an energy > 2 MeV, selected by an external trigger, and α particles from a ^{241}Am source with an energy of 5.49 MeV were used. The current pulses induced by particles penetrating the silicon diode are detected by a fast current amplifier with an input impedance $R_a = 50\ \Omega$, providing a gain of $G = 1000$. The pulses are recorded by a LeCroy digital oscilloscope used in averaging mode, to improve the signal-to-noise ratio. A summary of the characteristics of the standard float zone silicon detectors, at $\Phi = 0$, used in the present work is given in Table 1. The maximum fluence to which the detectors were exposed is also indicated in the Table.

Table 1: Characteristics at $\Phi = 0$ of the standard float zone detectors used in the present work. The detectors were irradiated by step of fluence up to 9.92×10^{13} n/cm^2 for M4, up to 7.5×10^{13} p/cm^2 for M18, M25, and M35, and up to 10.6×10^{13} p/cm^2 for P88. M49, M50, and M53 were not irradiated

Detector	Current pulse source	Thickness (μm)	N$_0$ (10^{11} cm^{-3})	ρ k$\Omega \times$ cm	Maximum fluence (cm^{-2})
M4 (1 cm^2)	α	317	-3.4	12.2	9.92×10^{13} n
M18 (1 cm^2)	α,β	309	-4.1	11	7.5×10^{13} p
M25 (1 cm^2)	α	308	-2.1	23	7.5×10^{13} p
M35 (1 cm^2)	α	508	-1.7	24	7.5×10^{13} p
M49 (1 cm^2)	β	301	-4.7	8.9	–
M50 (1 cm^2)	β	471	-1.8	22.8	–
M53 (1 cm^2)	β	223	-5.4	7.7	–
P88 (0.25 cm^2)	α	290	-18	2.5	10.6×10^{13} p
P189 (0.25 cm^2)	α	294	-18	2.5	10.6×10^{13} p
P304 (0.25 cm^2)	α	320	-7	6	10.6×10^{13} p

3.1 Data analysis

Using Ramo's theorem [4], it is possible to relate the movement of the charge carriers generated by an ionizing particle in a detector to the current they induce on the electrodes. The observed signal $[V(t)]$ is a convolution of the current $[I(t)]$ produced by all the individual charge carriers and the response from the system, which is simply an RC

circuit. The response of the system is a Gaussian with a characteristic time constant $\sigma = R_a C$, where C is the capacitance of the detector:

$$I(t) = \frac{18D_a t + r_0^2}{w r_0^2} \int_0^w (\mu_e n + \mu_h p) E \, dx \qquad (12)$$

$$V(t) = \frac{G R_a}{\sigma\sqrt{2\pi}} \sum_{e,h} \int_{-\infty}^{\infty} I(t') \exp\left(-\frac{(t-t')^2}{2\sigma^2}\right) dt' \; . \qquad (13)$$

It is necessary to know the concentration of the electrons and holes, as well as that of the electric field at every space-time coordinate. These quantities can be extracted from the system of partial differential equations introduced in Section 1. No analytical solution can be obtained, and the equations are therefore discretized using Gummel's decoupling scheme [5] to obtain a numerical solution (see Appendix). The quantities of interest are extracted by using the code MINUIT [6] to minimize the χ^2 obtained from fitting the numerical solutions of Eq. (13) to the experimental data obtained from the measurement of the current pulse response induced by α and β particles in the silicon detectors.

Figures 3 to 6 allow the transport of the charge carriers to be visualized by showing the location of the charge carriers as a function of the collection time, as well as the corresponding signals for an α particle incident on the front side (Figs. 3 and 6a), on the rear side (Figs. 4 and 6b) and for a β particle (Figs. 5 and 6c–d), respectively. For the α particles entering the rear side (n^+), the holes (h) drifting in the detector give the main contribution to the induced current. For the α particles entering the front side (junction side), the electrons (e) are the main contributors to the induced current. As hole mobility is smaller than electron mobility, the pulse from the rear side is longer. For the β particles, both electrons and holes contribute significantly to the current with a shorter signal for electrons because of their higher mobility.

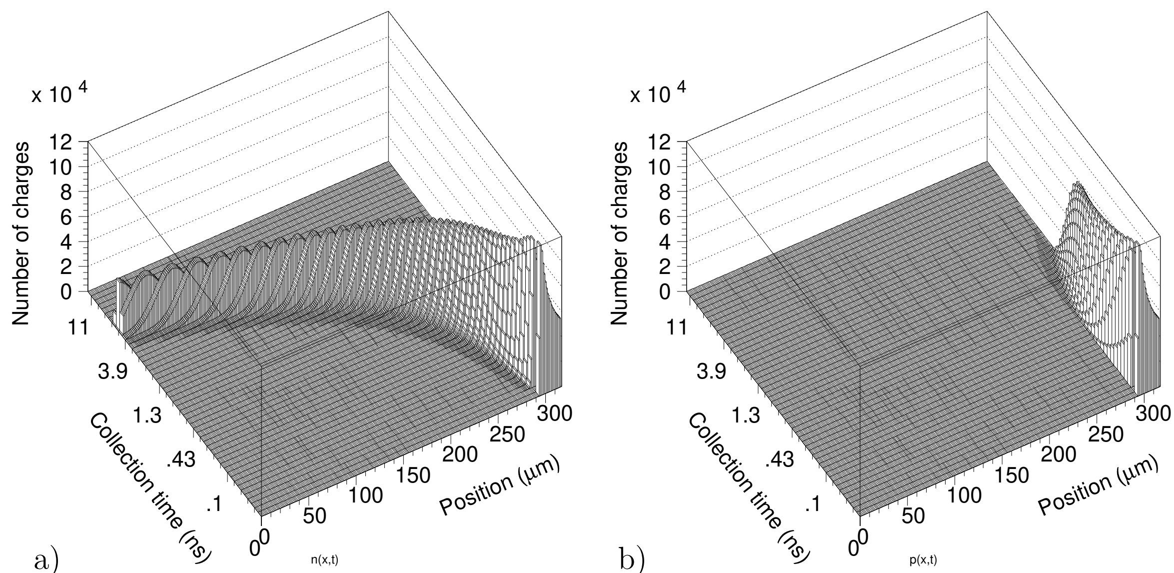

Figure 3: Charge transport for an alpha particle incident on the front side of a silicon diode: a) electron concentration, and b) hole concentration

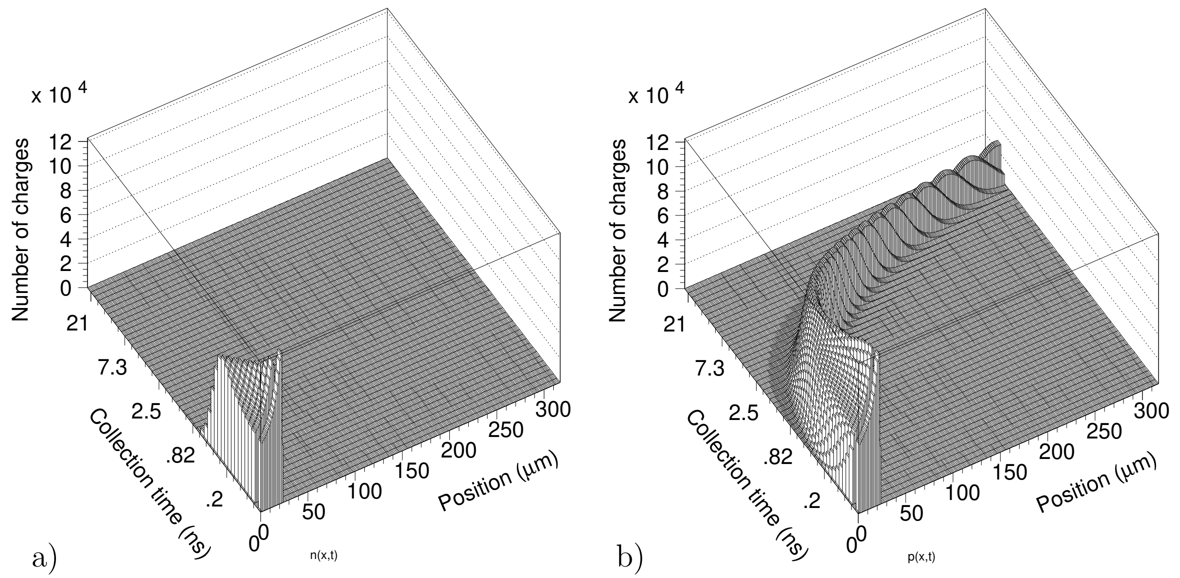

Figure 4: Charge transport for an alpha particle incident on the rear side of a silicon diode: a) electron concentration, and b) hole concentration

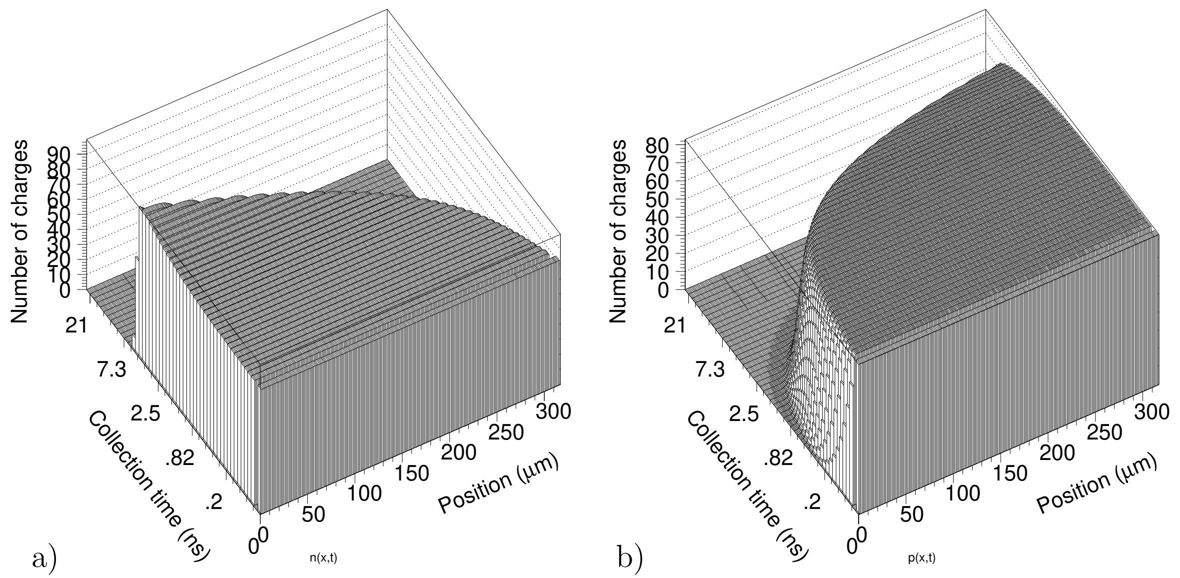

Figure 5: Charge transport for a beta particle incident on a silicon diode: a) electron concentration and b) hole concentration

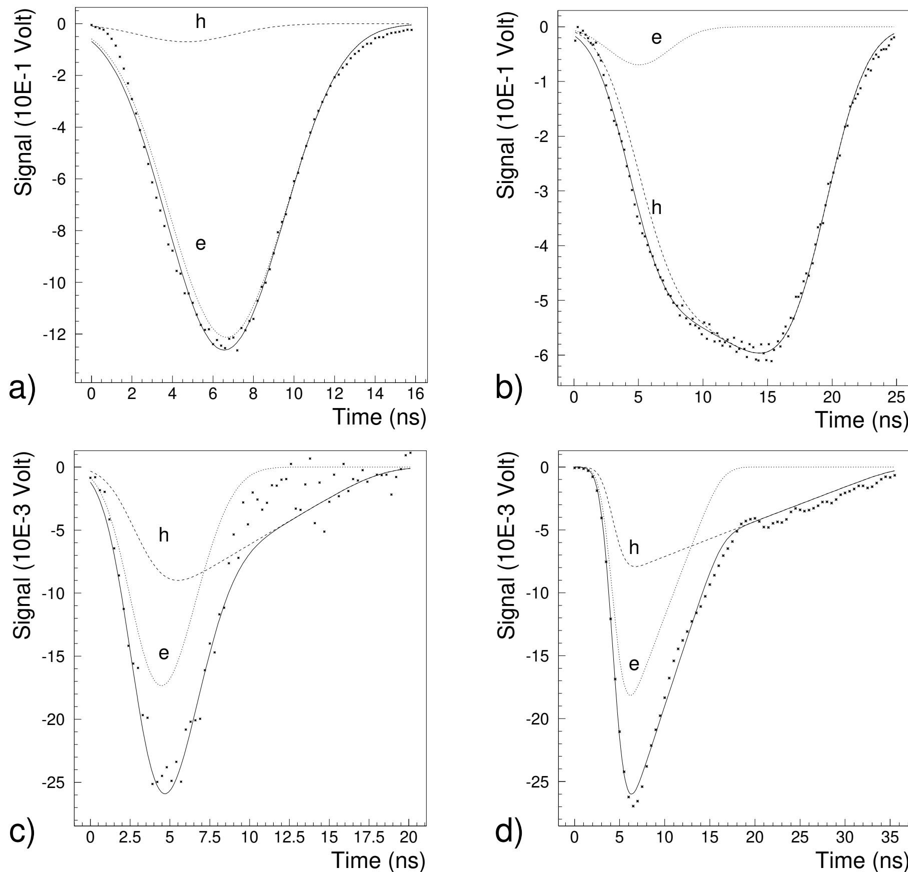

Figure 6: Fits (solid line) of the charge transport model to the current pulse response at $\Phi = 0$ for an α particle incident on the front side (a), on the rear side (b) for the M25 detector and for a relativistic electron for the M18 (c) and M50 (d) detectors; a bias voltage $V_b = 160$ V is applied in all cases. The individual electron (e) and hole (h) contributions are shown.

3.2 Electrical characteristics obtained from the charge transport model

3.2.1 Non-irradiated detectors ($\Phi = 0$)

Fits of the charge transport model to the current pulses induced by relativistic electrons and by α-particles either on the front side or the rear side are shown in Fig. 6. The model reproduces well the shape of the experimental data (α and β) and gives the values of the electron and hole mobilities reported in Table 2. The average mobilities achieved for electrons and holes are: $\mu_h = 492 \pm 9$ cm^2/Vs and $\mu_e = 1267 \pm 20$ cm^2/Vs, respectively.

3.2.2 Irradiated detectors and the necessity of a double junction

The defects induced by neutrons or protons in the silicon bulk act as generation-recombination centres, increasing the diode reverse current. These centres also act as electrically active defects (acceptors) that modify the initial effective impurity concentrations $N_{\rm eff}$ [7]. The results of the charge transport model fits to the experimental data permit the extraction of the value of $N_{\rm eff}$ as a function of the fluence (Fig. 7) and show that a silicon detector, initially of n-type, becomes apparently intrinsic around $\Phi_{\rm inv} \approx 5\times10^{12}$ n/p cm^{-2} ($\Phi_{\rm inv}$ is the value of the fluence at inversion) and inverts to an apparent p-type for higher fluences, with $N_{\rm eff}$ increasing with fluence:

$$\mathbf{N}_{\rm eff} = \mathbf{N}_0 \exp(-c\Phi) + b\Phi \ . \tag{14}$$

Table 2: Electron and hole mobilities of the various detectors extracted from the model fitted to β and α data at $\Phi = 0$

Detector	Current pulse source	μ_h ($cm^2 \times V^{-1} \times s^{-1}$)	μ_e ($cm^2 \times V^{-1} \times s^{-1}$)
M4	α	503.8 ± 2.2	1278 ± 15
M18	α, β	474.4 ± 2.4	1237 ± 15
M25	α	476.0 ± 2	1308 ± 28
M35	α	472.1 ± 3	1272 ± 5
M49	β	546 ± 11	1266 ± 24
M50	β	529 ± 13	1272 ± 20
M53	β	478 ± 12	1350 ± 20
P88	α	459.1 ± 4	1222 ± 20
P189	α	480 ± 20	1340 ± 27
P304	α	505 ± 15	1124 ± 22

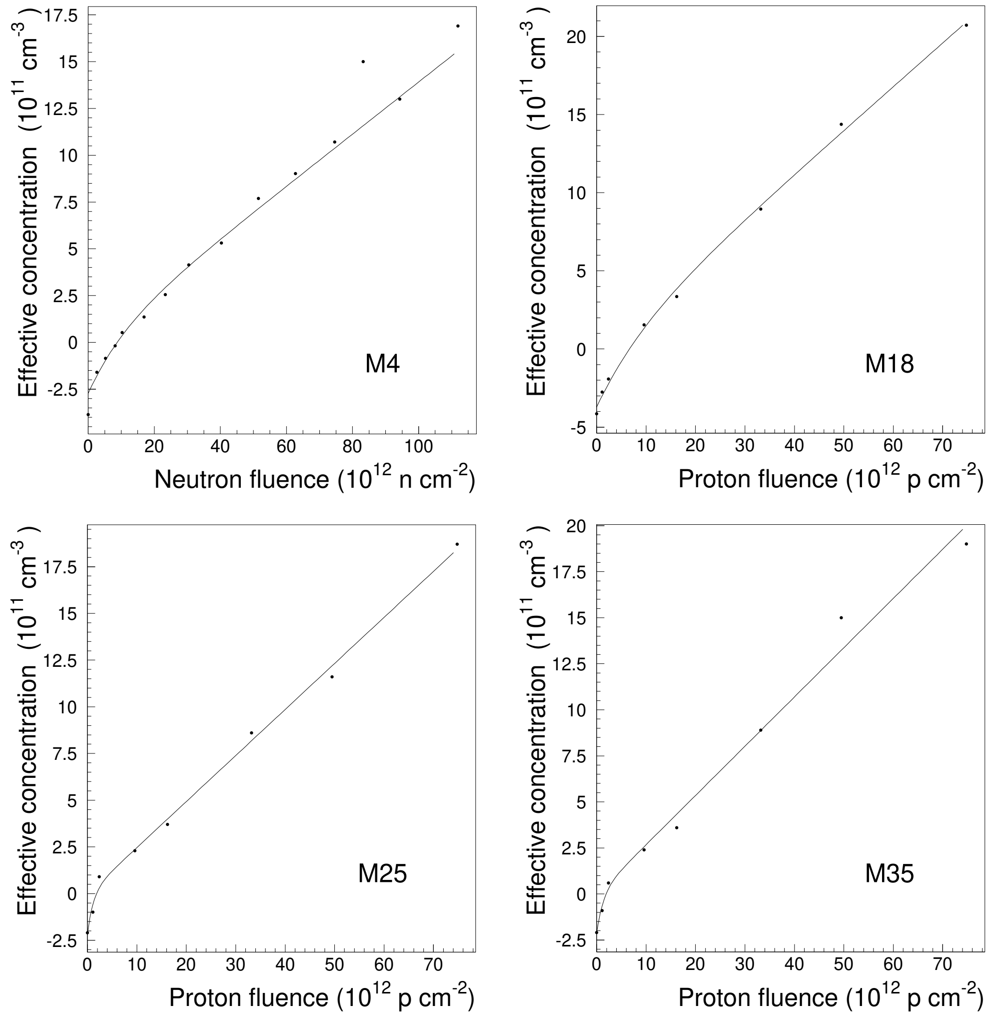

Figure 7: Evolution of the concentration of dopants (N_{eff}) of the M4, M18, M25 and M35 detectors as a function of fluence. The detectors with higher initial resistivities invert from n- to p-type at lower fluence values.

By using Eq. (14) to describe the evolution of $N_{\rm eff}$ with fluence, one obtains the results shown in Table 3. Correlated with the conduction-type inversion, the junction moves from the front side to the rear side. As a consequence, for a given bias voltage, the shape of the electric fields depends on the fluence level [Eq. (6)] as does the current induced by the moving charge carriers. The current slope is negative before irradiation, decreases up to $\Phi_{\rm inv}$, changes sign with the conduction-type inversion, and becomes more and more positive with increasing fluence. This is illustrated by Figs. 8 and 9 which show the results of the fit of the charge transport model to the current pulse responses of α particles incident on the front side (Fig. 8) and on the rear side (Fig. 9) of the M18 detector for successive proton irradiation levels.

Figures 10 to 13 show the results of the fit of the charge transport model to the current pulse responses of α particles incident on the front side and on the rear side of the M4 detector for successive neutron irradiation levels.

One problem with the simple p–n$^+$ junction used after type-inversion is that the mobilities keep on decreasing continuously with increasing fluence. Although $\mu_h = 474.4$ cm^2/Vs and $\mu_e = 1237$ cm^2/Vs at $\Phi = 0$ for the M18 detector, the values of the mobilities for this detector drop to $\mu_h = 338$ cm^2/Vs and $\mu_e = 700$ cm^2/Vs at a fluence of $\Phi = 7.5 \times 10^{13}$ p/cm^2, without showing any sign of saturation. In addition, the charge transport model reproduces the experimental data for the M4 detector poorly (Figs. 11 and 13). The starting values of $\mu_h = 503.8$ cm^2/Vs and $\mu_e = 1278$ cm^2/Vs at $\Phi = 0$ for M4 drop to $\mu_h = 429$ cm^2/Vs and $\mu_e = 790$ cm^2/Vs for a fluence of $\Phi = 9.96 \times 10^{13}$ n/cm^2 (Figs. 11 and 13).

Table 3: Parameters describing the evolution of the effective concentration of dopants with fluence

Detector	N$_0$ 10^{11} cm^{-3}	b 10^{-2}/(particles cm)	c 10^{-11} cm^2/particles	$\Phi_{\rm inv}$ 10^{12} cm^{-2}
M4	−2.7	1.4	9	≈ 8 (n)
M18	−3.7	2.8	10	≈ 7 (p)
M25	−2.2	2.5	85	≈ 2 (p)
M35	−2.2	2.7	76	≈ 2 (p)

The poor agreement between model and data appears after the inversion point as shown by Figs. 11 and 13 for the M4 detector. In order to remove this discrepancy, we have modified the electric field after inversion by introducing a 15 μm n-type region near the p$^+$ contact ($x_a < x < w$). The electric field at $t = 0$ in the detector is then approximated by (Fig. 14):

$$E(x,0) = \begin{cases} \frac{-qN_a}{\epsilon}(x - x_a) + \frac{V_b - V_{d2}}{w} & \text{for } 0 < x \le x_a \\ \\ \frac{qN_d}{\epsilon}(x - x_a) + \frac{V_b - V_{d2}}{w} & \text{for } x_a \le x < w \, , \end{cases} \tag{15}$$

where V_{d2} is the full depletion bias. This concept of a double junction can also be found in Refs. [8, 9, 10]. The introduction of this thin n-type region after type inversion, allows the charge transport model to reproduce the data (Figs. 15 and 16) up to the highest value of fluence. As for an alpha particle incident on the front side most of the charge is located around 20 μm from the front side, the introduction of a 15 μm double junction has no significant influence on the signal (comparing Figs. 11 and 16).

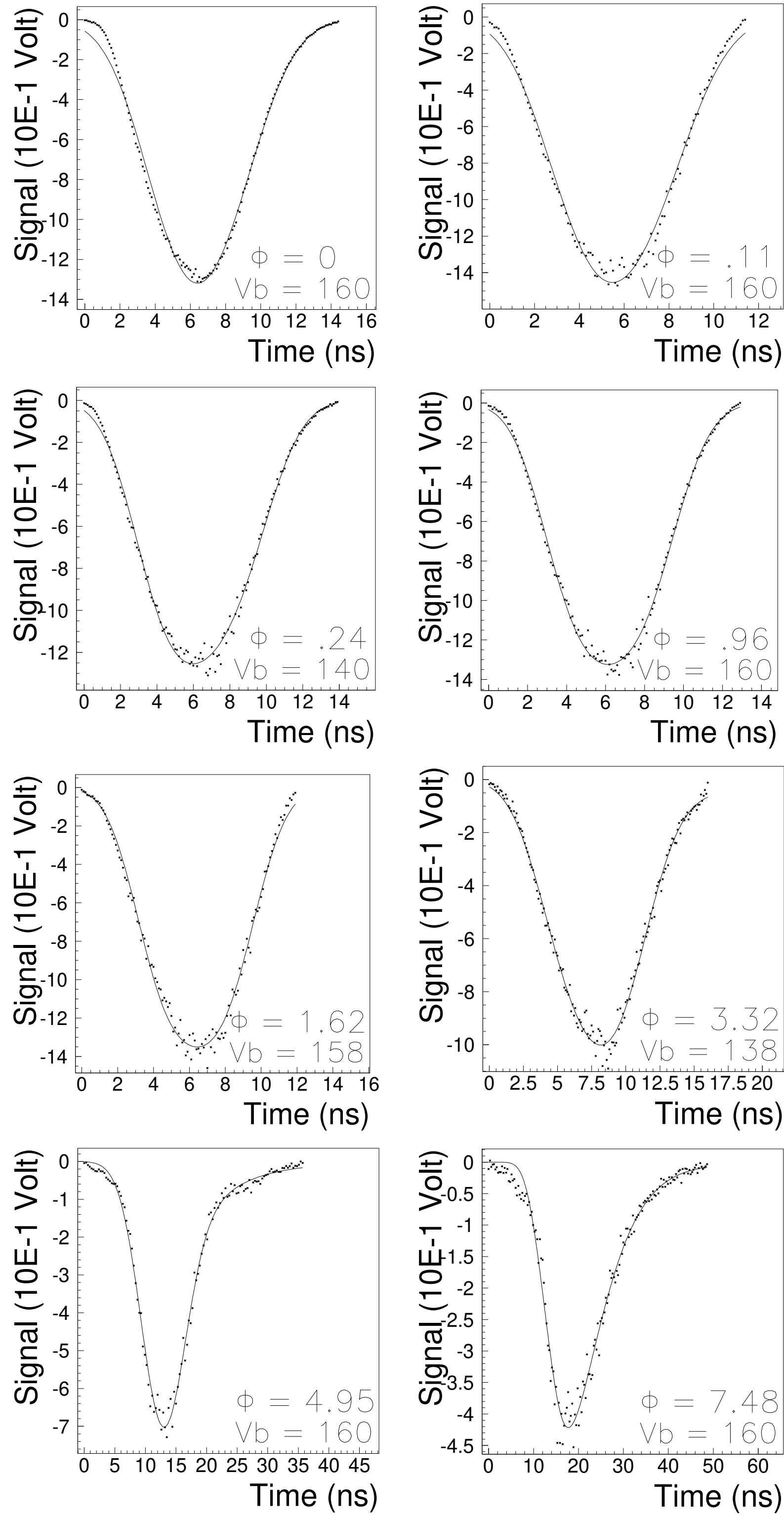

Figure 8: Fits (solid line) of the current pulse responses to α particles incident on the front side of the M18 detector for successive levels of fluence Φ up to 7.5×10^{13} p/cm^2 (Φ in 10^{13} p/cm^2, V_b the applied voltage in volts)

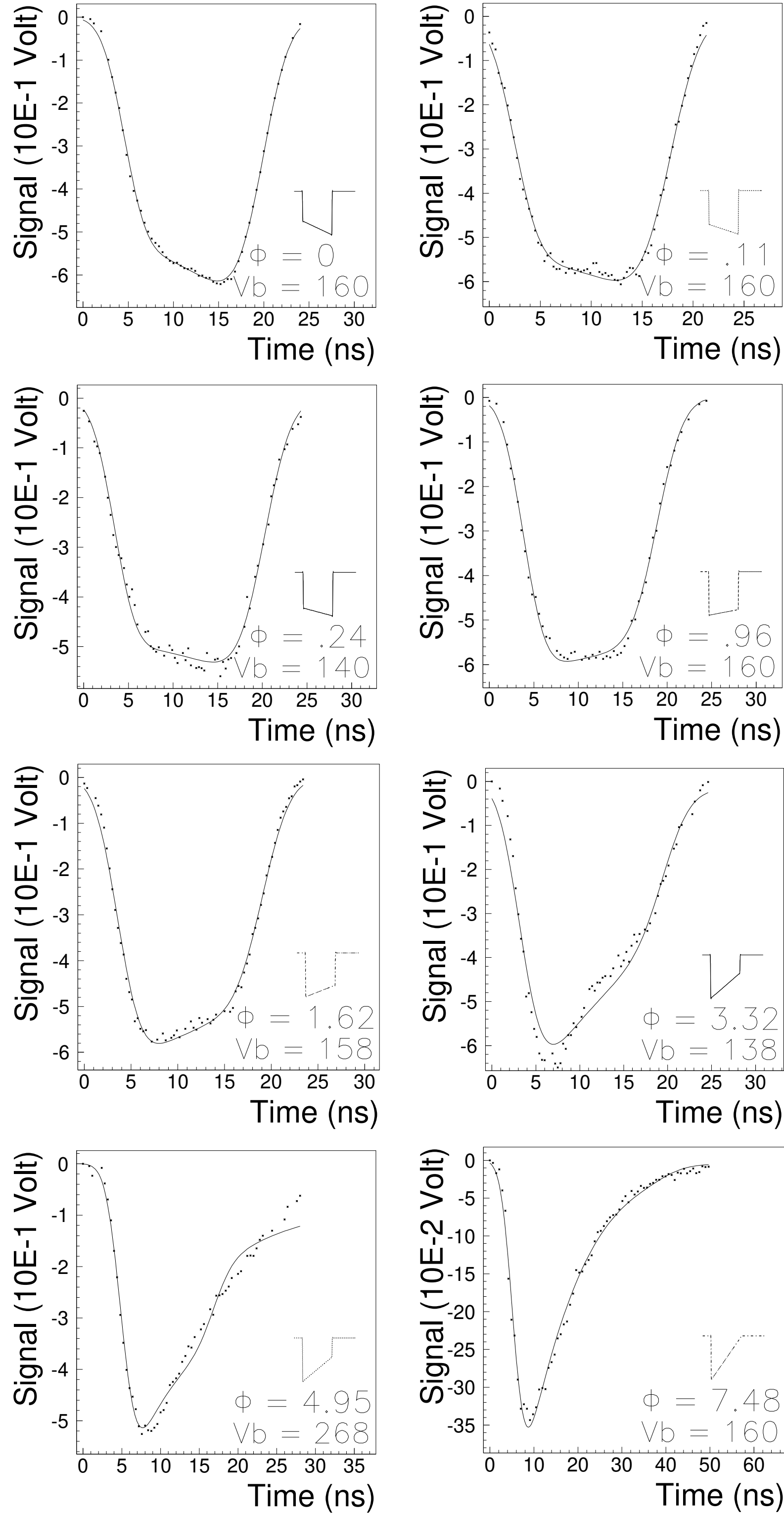

Figure 9: Fits (solid line) of the current pulse responses to α particles incident on the rear side of the M18 detector for successive levels of fluence Φ up to 7.5×10^{13} p/cm^2 (Φ in 10^{13} p/cm^2, V_b the applied voltage in volts). The smaller graphs show the evolution of the electrical field $[-E(x,0)]$.

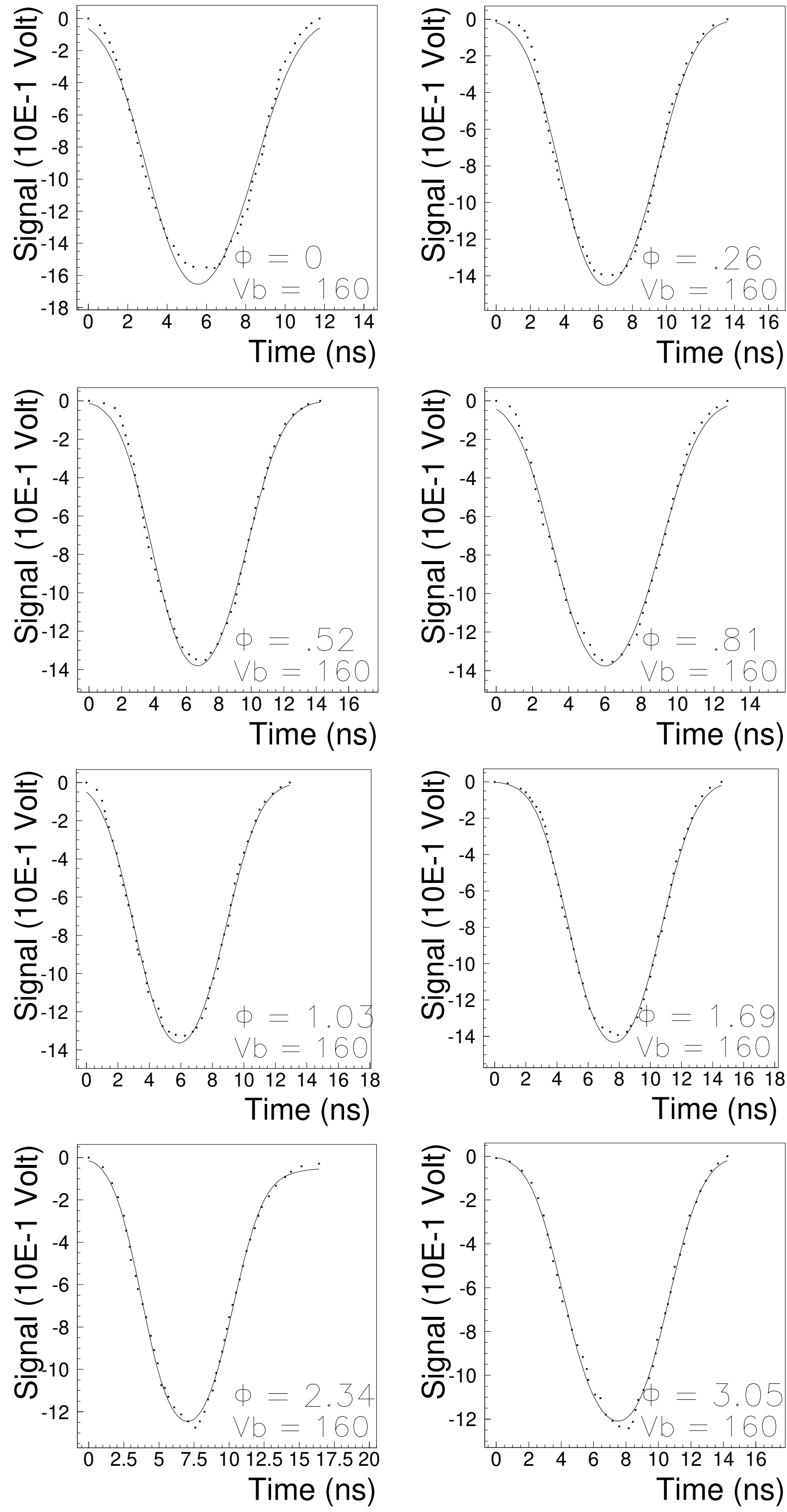

Figure 10: Fits (solid line) of the current pulse responses to α particles incident on the front side of the M4 detector for successive levels of fluence Φ up to 3.05×10^{13} n/cm^2 (Φ in 10^{13} n/cm^2, V_b the applied voltage in volts)

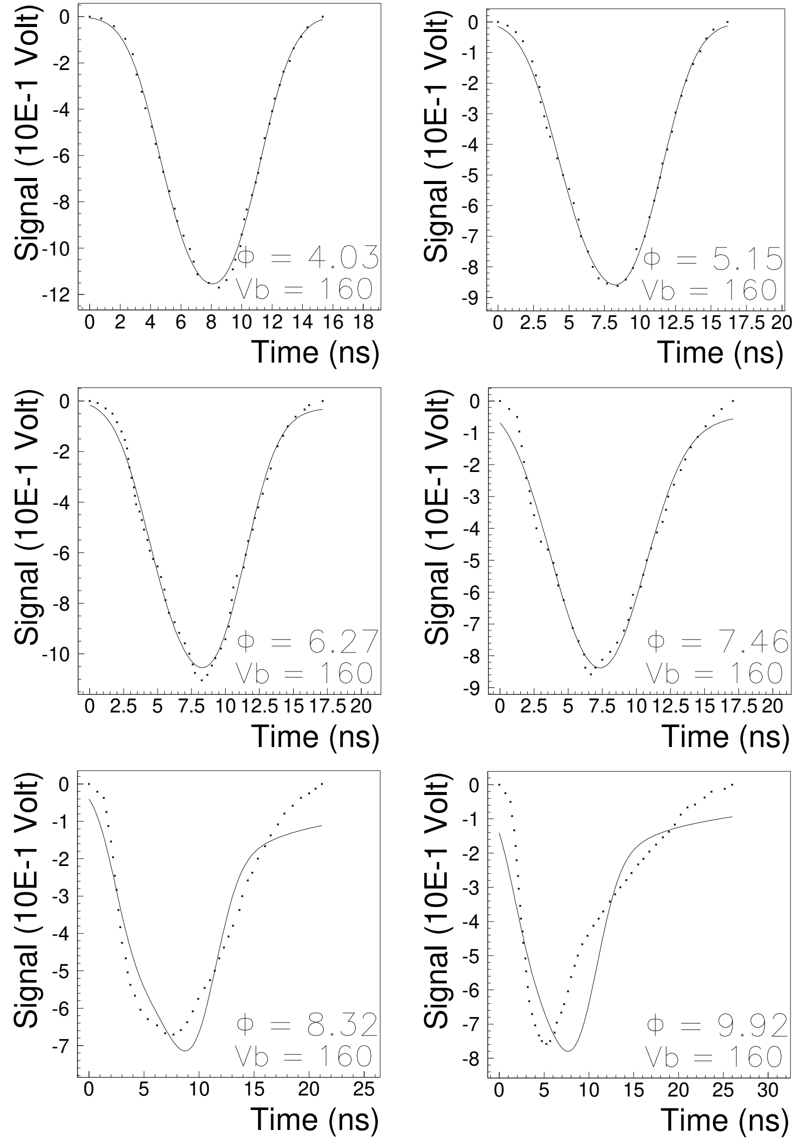

Figure 11: Fits (solid line) of the current pulse responses to α particles incident on the front side of the M4 detector for successive levels of fluence between $\Phi = 4.03$ and 9.92×10^{13} n/cm^2 (Φ in 10^{13} n/cm^2, V_b the applied voltage in volts)

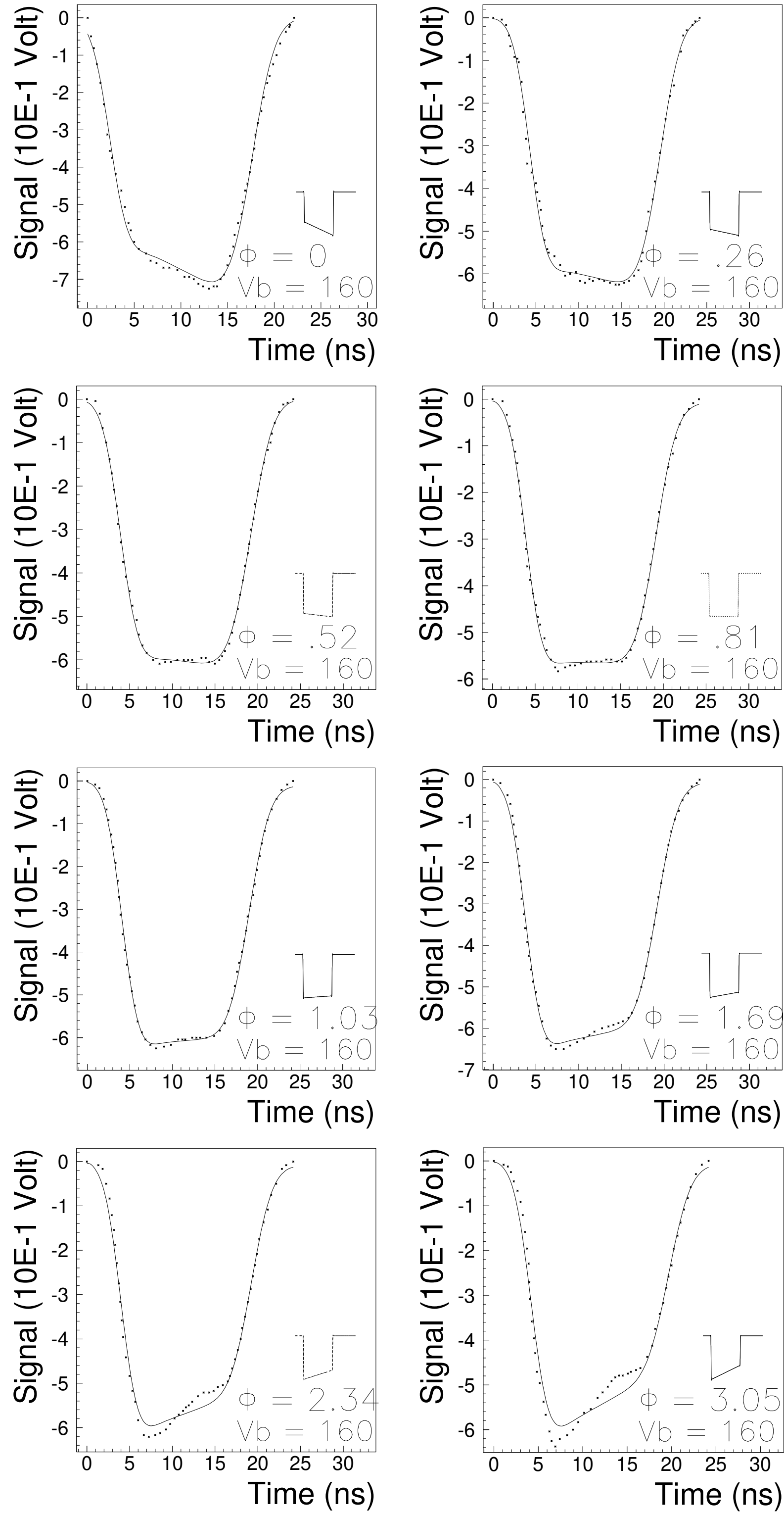

Figure 12: Fits (solid line) of the current pulse responses to α particles incident on the rear side of the M4 detector for successive levels of fluence Φ up to 3.05×10^{13} n/cm^2 (Φ in 10^{13} n/cm^2, V_b the applied voltage in volts). The smaller graphs show the evolution of the electrical field $[-E(x,0)]$.

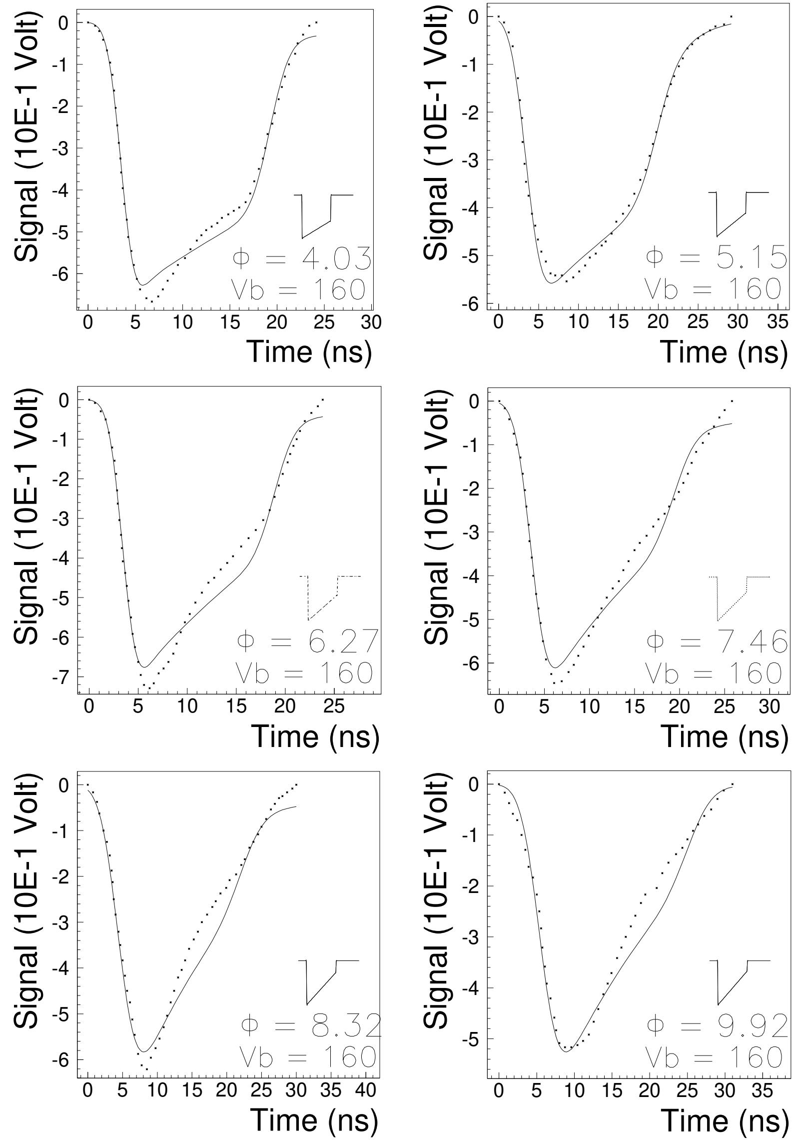

Figure 13: Fits (solid line) of the current pulse responses to α particles incident on the rear side of the M4 detector for successive levels of fluence between $\Phi = 4.03$ and 9.92×10^{13} n/cm^2 (Φ in 10^{13} n/cm^2, V_b the applied voltage in volts). The smaller graphs show the evolution of the electrical field $[-E(x, 0)]$.

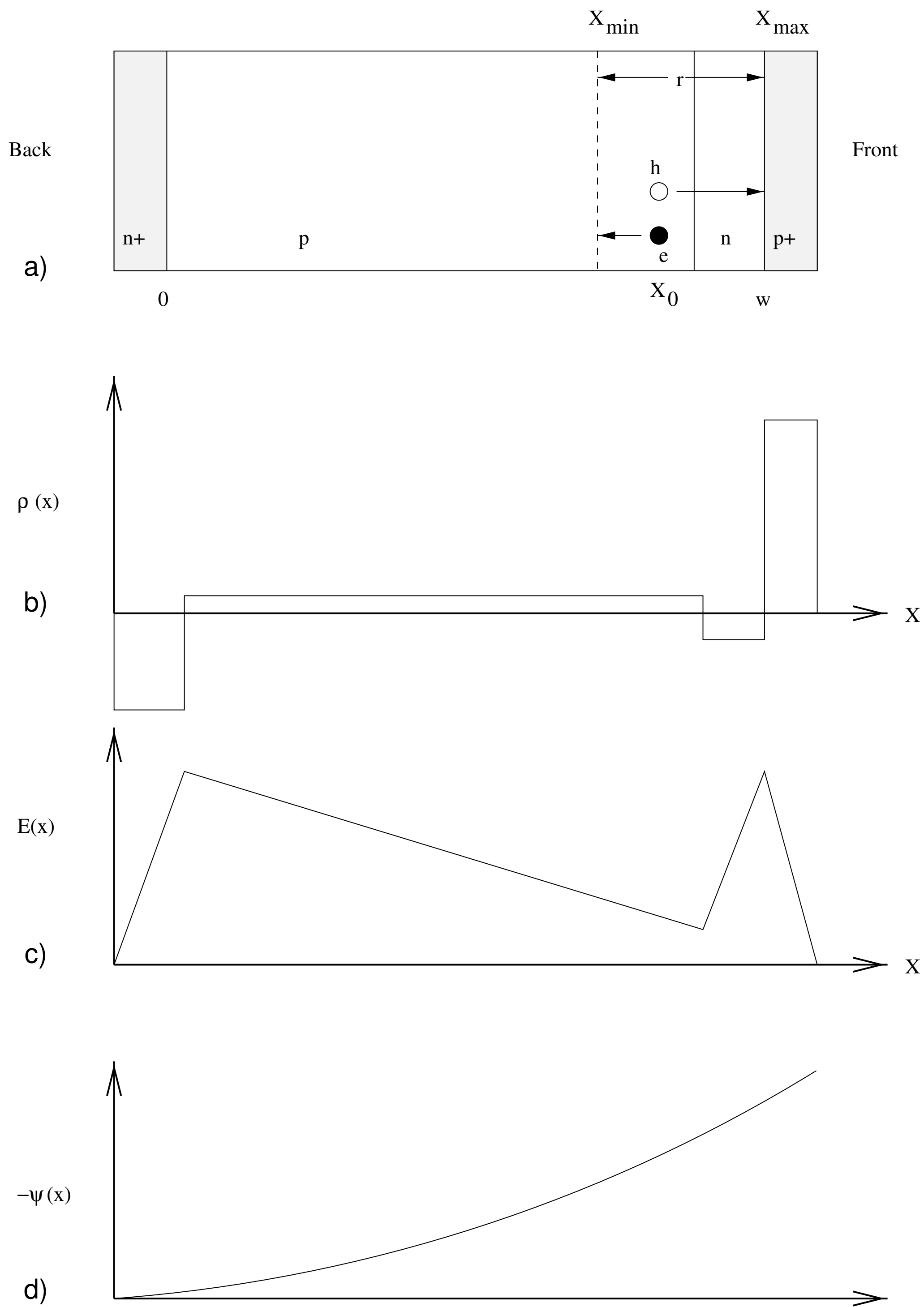

Figure 14: a) Representation of a $p^+ - n - p - n^+$ diode, b) its dopant profile (ρ), c) its electric field (E), and d) its electrostatic potential (ψ)

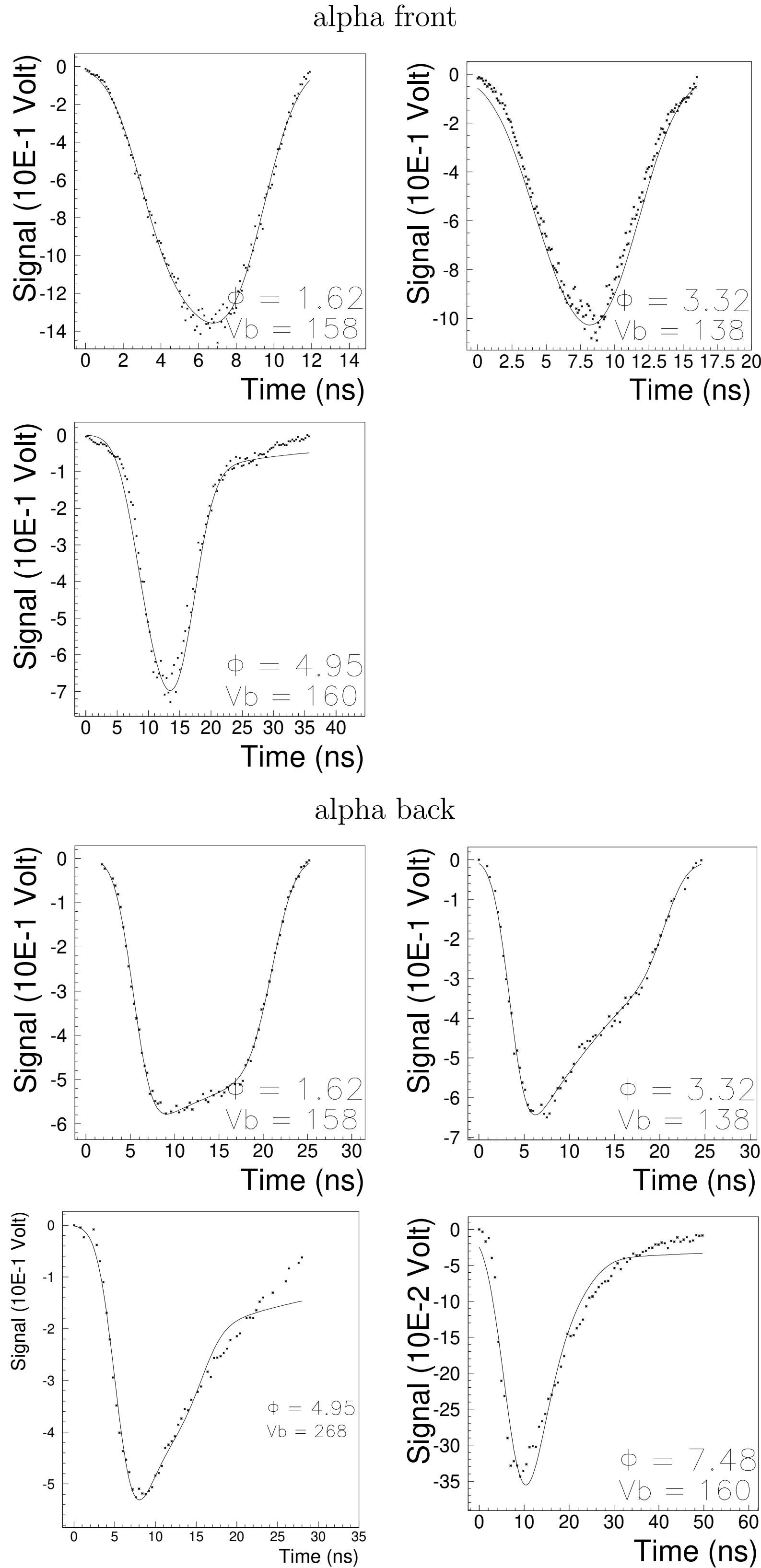

Figure 15: Fits for a $p^+{-}n{-}p{-}n^+$ diode with a double junction (resulting from the introduction of the 15 μm n-type junction on the p^+ side after inversion) for the M18 detector, with α particles on the front side (alpha front) and on the rear side (alpha back) for successive levels of fluence $\Phi = 1.62 \times 10^{13}$ p/cm^2 up to $\Phi = 7.5 \times 10^{13}$ p/cm^2 (Φ in 10^{13} p/cm^2, V_b the applied voltage in volts)

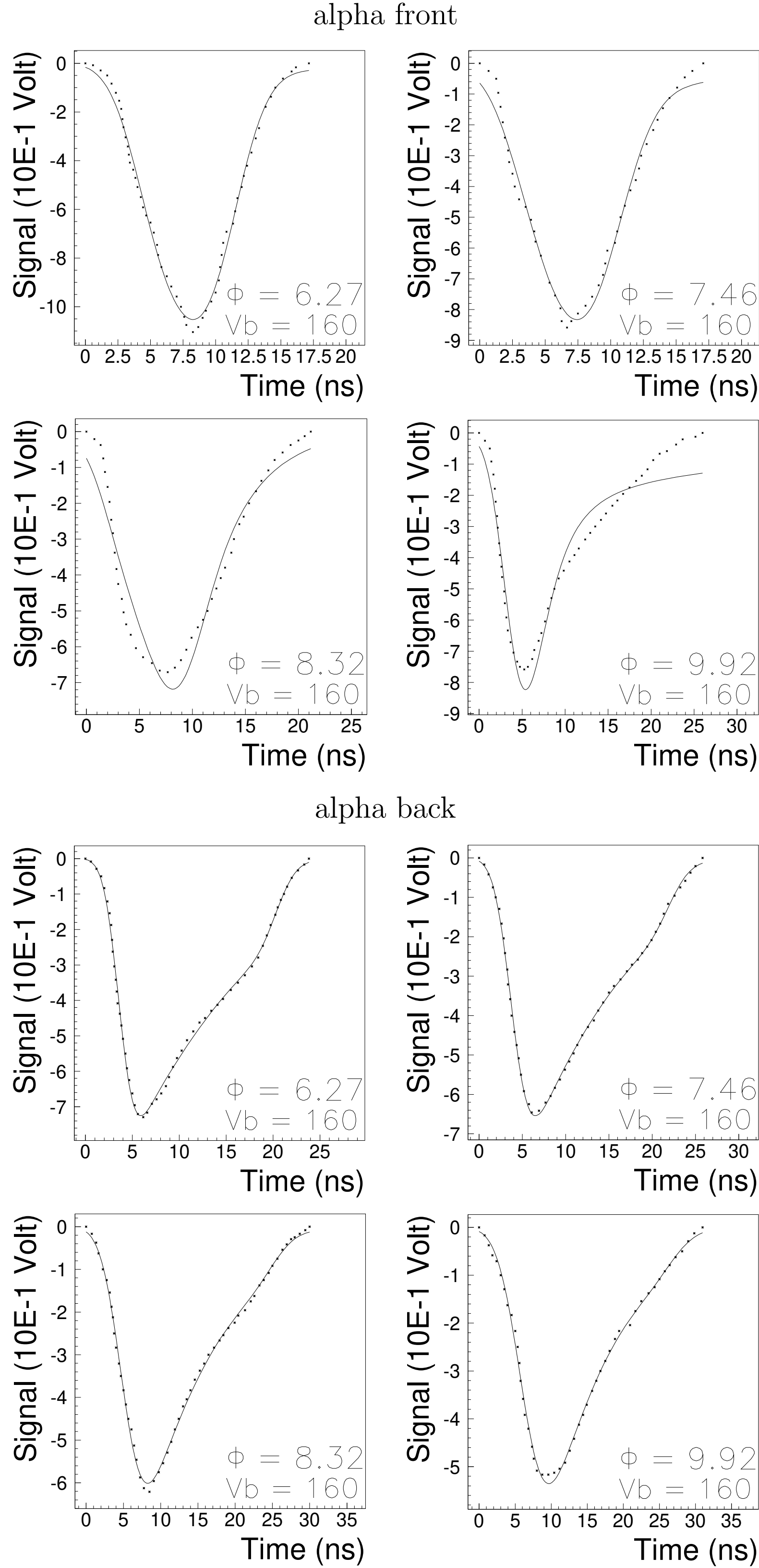

Figure 16: Fits for a $p^+{-}n{-}p{-}n^+$ diode with a double junction (resulting from the introduction of the 15 μm n-type junction on the p^+ side after inversion) for the M4 detector, with α particles on the front side (alpha front) and on the rear side (alpha back) for successive levels of fluence $\Phi = 6.27 \times 10^{13}$ n/cm^2 up to $\Phi = 10^{14}$ n/cm^2 (Φ in 10^{13} n/cm^2, V_b the applied voltage in volts)

Moreover, the introduction of the 15 μm n-type region close to the p^+ contact modifies the dependence of the extracted mobilities on the fluence. The mobility now tends, after an initial decrease, towards a saturation value ($\mu_{\mathrm{sat}_{e,h}}$) for the electrons and holes at $\Phi > \Phi_{\mathrm{inv}}$ (the situation for the neutron-irradiated M4 detector is shown in Fig. 17 and for the proton-irradiated M18 detector in Fig. 19). The initial decrease is described by:

$$\mu_{e,h} = a_{e,h} - b_{e,h} \times \Phi \ . \tag{16}$$

The saturation values ($\mu_{\mathrm{sat}_{e,h}}$) for $\Phi > \Phi_{\mathrm{inv}}$ and the coefficients $a_{e,h}$ and $b_{e,h}$ are given in Table 4.

Table 4: Parameters describing the evolution of the mobilities with fluence

Detector	a_h cm^2/Vs	a_e cm^2/Vs	b_h cm^4/(particles Vs)	b_e cm^4/(particles Vs)	μ_{sat_h} cm^2/Vs	μ_{sat_e} cm^2/Vs
M4	503	1200	4.7×10^{-13}	46×10^{-13}	475	990
M18	473	1195	4.6×10^{-13}	124×10^{-13}	460	1030
M25	472	1295	6.9×10^{-13}	95×10^{-13}	462	990
M35	490	1233	8.0×10^{-13}	115×10^{-13}	460	1000

Figures 18 and 20 show that for neutron- and proton-irradiated detectors, respectively, as the fluence and thus the number of traps increases, the charge carrier lifetimes due to trapping, decrease. The integration of Eq. (13) over the collection time allows the collected charge to be determined, and thus by comparing the results obtained using the trapping lifetime extracted at the maximum fluences with those obtained if no trapping had occurred, a collection deficit of 13% is calculated. This is in agreement with the 12% obtained from charge collection efficiency (CCE) measurements made with β particles [11].

4 CONCLUSIONS

A model describing the transport of charge carriers deposited in silicon detectors by ionizing particles is presented. It allows the current pulse response of non-irradiated and irradiated detectors induced by α and β particles to be reproduced up to fluences around the n- to p-type inversion ($\Phi \approx \Phi_{\mathrm{inv}}$) using a simple $p^+ - n - n^+$ diode. Beyond inversion ($\Phi > \Phi_{\mathrm{inv}}$), a small n-type region 15 μm deep is introduced on the p^+ side of the detector. The introduction of this region modifies the electric field after inversion and permits the charge transport model to reproduce the experimental data up to fluences of 10^{14} particles/cm^2.

This model gives mobilities which decrease linearly up to fluences of around 5×10^{13} particles/cm^2 and beyond, converging to saturation values of about 1000 cm^2/Vs and 460 cm^2/Vs for electrons and holes, respectively.

The charge carrier lifetime degradation due to trapping is responsible for a charge collection deficit of about 13%, in agreement with the charge collection deficit measured directly with β particles.

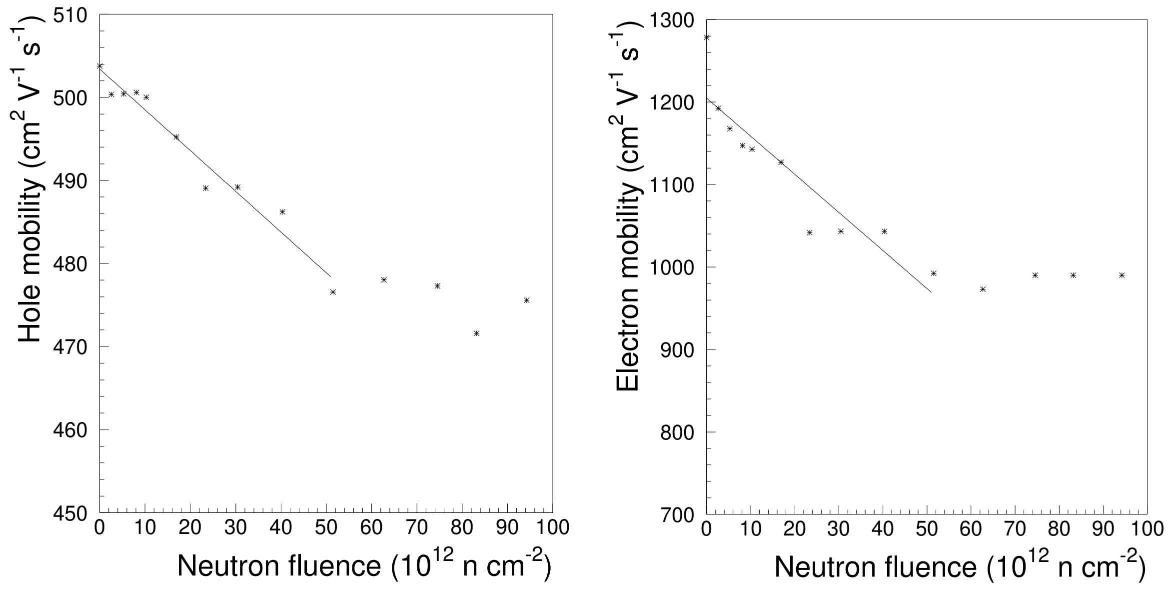

Figure 17: Evolution of the mobilities for the M4 detector as a function of fluence

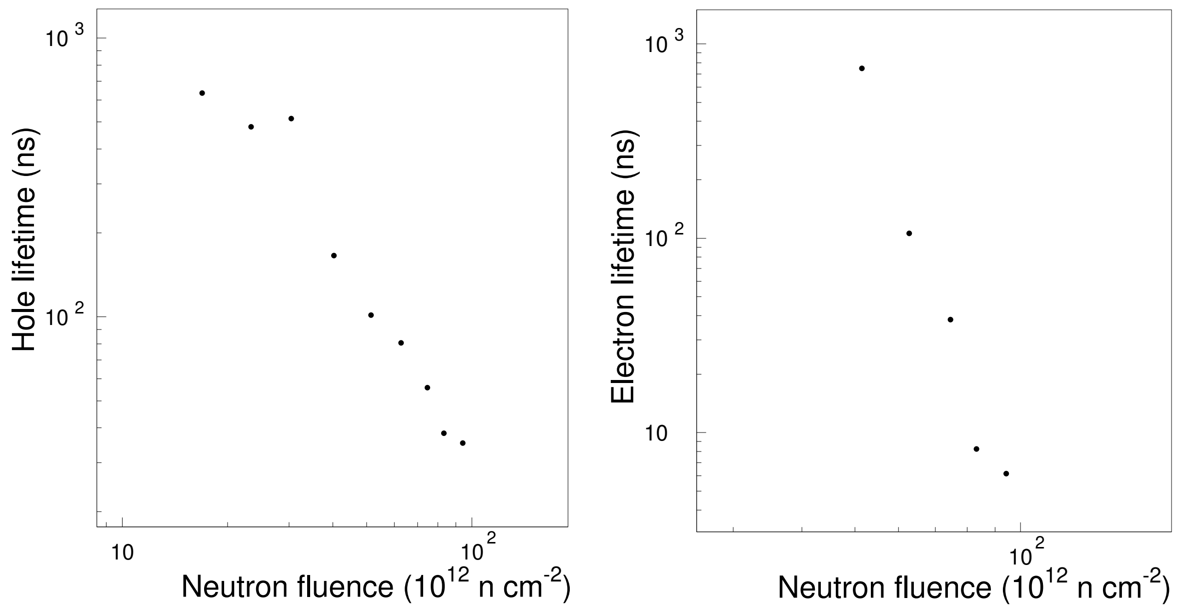

Figure 18: Evolution of the carrier lifetime due to trapping of the M4 detector as a function of fluence

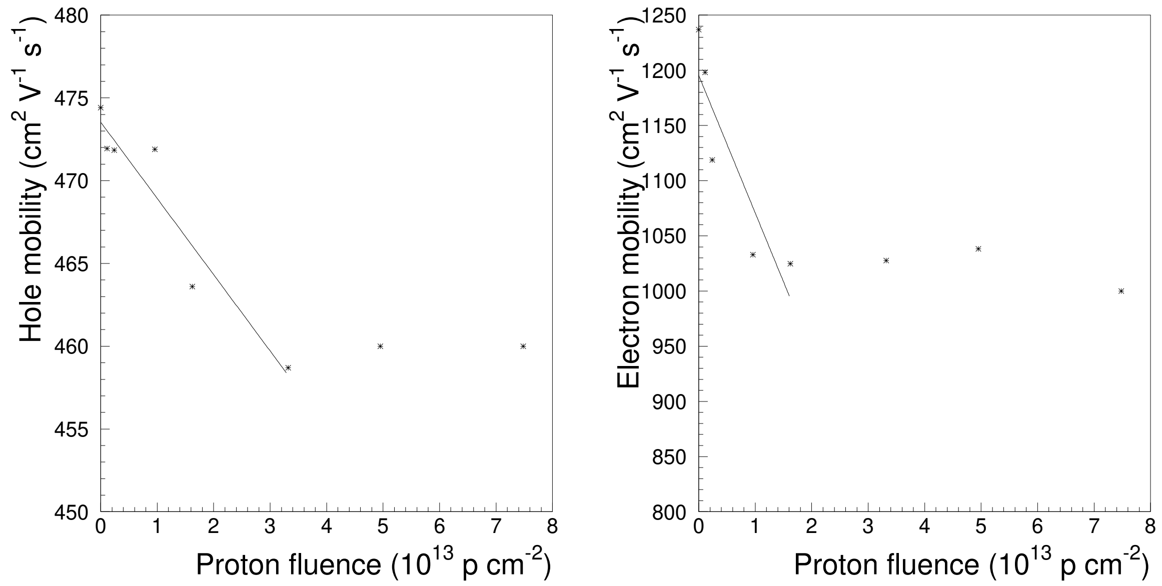

Figure 19: Evolution of the mobilities for the M18 detector as a function of fluence

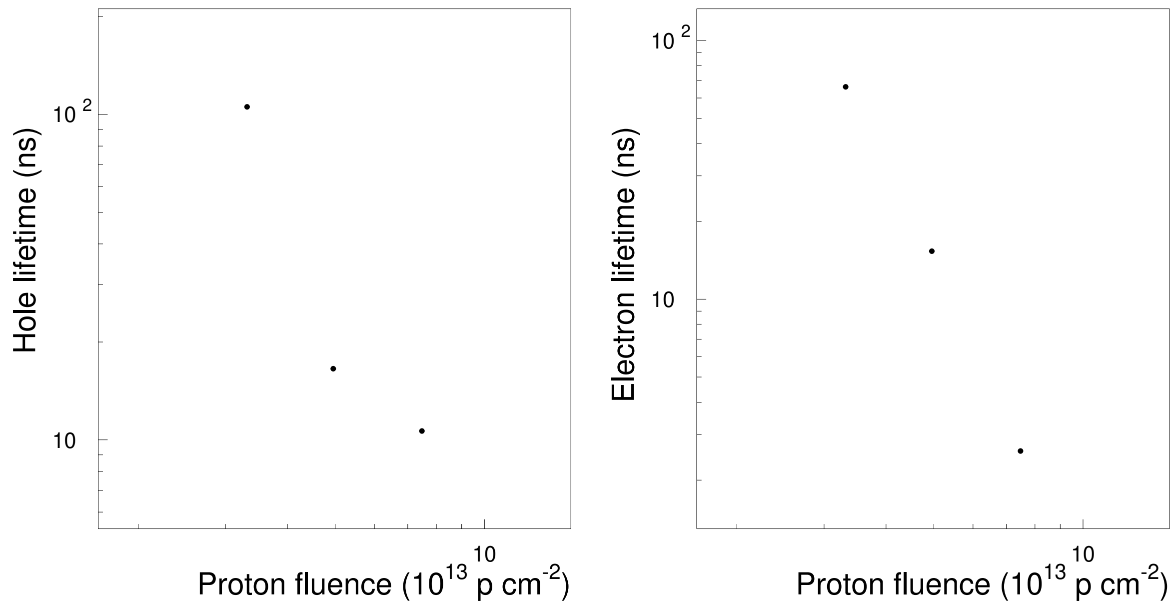

Figure 20: Evolution of the carrier lifetime due to trapping of the M18 detector as a function of fluence

APPENDIX

As the concentration of carriers is a quantity that changes rapidly, it is better to express it in terms of the quasi-Fermi potentials (Φ_c and Φ_{c_t}) for numerical purposes:

$$c = n_i e^{\pm q(\psi - \Phi_c)/k_B T} \qquad \text{and} \qquad c_t = n_i e^{\pm q(\psi - \Phi_{c_t})/k_B T} \ . \tag{A.1}$$

The variables used in the previous equations each have their own characteristic scale. The first step to resolve them numerically consists of making them dimensionless. Table A.1 shows the values used (from De Mari [12]).

Table A.1: List of normalization factors

Quantity	Symbol	Value
x	X_0	$\sqrt{\varepsilon k_B T / q^2 n_i}$
$\psi, \Phi_n, \Phi_p, \Phi_{n_t}, \Phi_{p_t}$	ψ_0	$k_B T/q$
$n, n_t, p, p_t, N_{\text{eff}}$	N_0	n_i
D_n, D_p, D_a	D_0	$1 \text{ cm}^2 \text{ s}^{-1}$
$t, \tau_{re}, \tau_{rh}, \tau_{ce}, \tau_{ch}$	t_0	X_0^2/D_0
U_{SRH}, R, g	U_0	$D_0 N_0 / X_0^2$

This allows the problem to be reformulated as:

$$\frac{\partial^2 \psi}{\partial x^2} = -(-N_{\text{eff}} - n + p - n_t + p_t) \tag{A.2}$$

$$\frac{\partial c}{\partial t} = D \frac{\partial}{\partial x}\left(-c\frac{\partial \psi}{\partial x} \pm \frac{\partial c}{\partial x}\right) - U_{SRH} + g - Rc - \frac{\partial c_t}{\partial t} \tag{A.3}$$

$$\frac{\partial c_t}{\partial t} = \frac{c}{\tau_{tc}} - \frac{c_t}{\tau_{dc}} - Rc_t \ . \tag{A.4}$$

The simultaneous solution of the system of coupled equations [Eqs. (A.2) to (A.4)] can be simplified by using an iterative method, where the equations are solved one after the other. The scheme proposed by Gummel [5] consists in making the hypothesis that the quasi-Fermi potentials are constant between each iteration, which allows the equations to be decoupled. At the iteration k, the variables are ψ^k, n^k, p^k, n_t^k et p_t^k. By defining:

$$\Delta^k \psi = \psi^k - \psi^{k-1} \tag{A.5}$$

$$\bar{c}_{k-1} = c^{k-1} e^{\Delta^k \psi} \ , \tag{A.6}$$

Poisson's equation can be rewritten as:

$$\frac{\partial^2 \psi}{\partial x^2} = -(-N_{\text{eff}} - \bar{n}_{k-1} + \bar{p}_{k-1} - \bar{n}_{tk-1} + \bar{p}_{tk-1}) \ . \tag{A.7}$$

By expanding the exponentials, Poisson's equation becomes a linear function of the electrostatic potential:

$$\frac{\partial^2 \psi}{\partial x^2} = \Big(N_{\text{eff}} + (n^{k-1} + n_t^{k-1})(1 + \Delta^k \psi) - (p^{k-1} + p_t^{k-1})(1 - \Delta^k \psi)\Big) \ . \tag{A.8}$$

The discretization of Poisson's equation is obtained by rewritting the electrostatic potential as:

$$\begin{aligned}\psi(x) &= \frac{(x-x_i)(x-x_{i+1})}{(x_{i-1}-x_i)(x_{i-1}-x_{i+1})}\psi_{i-1} + \frac{(x-x_{i-1})(x-x_{i+1})}{(x_i-x_{i-1})(x_i-x_{i+1})}\psi_i \\ &\quad + \frac{(x-x_{i-1})(x-x_i)}{(x_{i+1}-x_{i-1})(x_{i+1}-x_i)}\psi_{i+1} \; . \end{aligned} \tag{A.9}$$

This allows one to obtain:

$$\psi''(x_i) = \psi_i'' = \frac{2\psi_{i-1}}{h_{i-1}(h_i+h_{i-1})} - \frac{2\psi_i}{h_i h_{i-1}} + \frac{2\psi_{i+1}}{h_i(h_i+h_{i-1})} \; , \tag{A.10}$$

where the step is defined as:

$$h_i = x_{i+1} - x_i \; . \tag{A.11}$$

Thus for a constant step:

$$\psi_i'' = \frac{\psi_{i-1} - 2\psi_i + \psi_{i+1}}{h^2} \; . \tag{A.12}$$

In matrix form Poisson's equation will be:

$$\begin{aligned}
&\frac{1}{h^2}\begin{pmatrix} -2 & 1 & & & & & \\ 1 & -2 & 1 & & & & \\ & 1 & -2 & 1 & & & \\ & & & \cdot & & & \\ & & & & \cdot & & \\ & & & & & \cdot & \\ & & & & & 1 & -2 \end{pmatrix}\begin{pmatrix} \psi_1^k \\ \psi_2^k \\ \psi_3^k \\ \cdot \\ \cdot \\ \cdot \\ \psi_n^k \end{pmatrix} \\
&= \begin{pmatrix} n_1^{k-1} + n_{t1}^{k-1} + p_1^{k-1} + p_{t1}^{k-1} \\ n_2^{k-1} + n_{t2}^{k-1} + p_2^{k-1} + p_{t2}^{k-1} \\ n_3^{k-1} + n_{t3}^{k-1} + p_3^{k-1} + p_{t3}^{k-1} \\ \cdot \\ \cdot \\ \cdot \\ n_n^{k-1} + n_{tn}^{k-1} + p_n^{k-1} + p_{tn}^{k-1} \end{pmatrix}^T \begin{pmatrix} \psi_1^k \\ \psi_2^k \\ \psi_3^k \\ \cdot \\ \cdot \\ \cdot \\ \psi_n^k \end{pmatrix} + \begin{pmatrix} n_1^{k-1} + n_{t1}^{k-1} \\ n_2^{k-1} + n_{t2}^{k-1} \\ n_3^{k-1} + n_{t3}^{k-1} \\ \cdot \\ \cdot \\ \cdot \\ n_n^{k-1} + n_{tn}^{k-1} \end{pmatrix}^T \begin{pmatrix} 1-\psi_1^{k-1} \\ 1-\psi_2^{k-1} \\ 1-\psi_3^{k-1} \\ \cdot \\ \cdot \\ \cdot \\ 1-\psi_n^{k-1} \end{pmatrix} \\
&- \begin{pmatrix} p_1^{k-1} + p_{t1}^{k-1} \\ p_2^{k-1} + p_{t2}^{k-1} \\ p_3^{k-1} + p_{t3}^{k-1} \\ \cdot \\ \cdot \\ \cdot \\ p_n^{k-1} + p_{tn}^{k-1} \end{pmatrix}^T \begin{pmatrix} 1+\psi_1^{k-1} \\ 1+\psi_2^{k-1} \\ 1+\psi_3^{k-1} \\ \cdot \\ \cdot \\ \cdot \\ 1+\psi_n^{k-1} \end{pmatrix} - \begin{pmatrix} -N_{\mathrm{eff}} + \psi_0^k/h^2 \\ -N_{\mathrm{eff}} \\ -N_{\mathrm{eff}} \\ \cdot \\ \cdot \\ \cdot \\ -N_{\mathrm{eff}} + \psi_{n+1}^k/h^2 \end{pmatrix}
\end{aligned} \tag{A.13}$$

which is an equation of the form

$$(A_\psi - IB_\psi)\vec{\psi} = C_\psi\vec{\psi} = D_\psi \; , \tag{A.14}$$

where C_ψ is a tridiagonal matrix. Special methods exist to solve such equations efficiently. The method used here is a Gaussian elimination with row interchanges implemented in the CERN library under the name DBEQN [13].

The non-linearity of the generation-recombination term is removed by evaluating the function in terms of n^{k-1} and p^{k-1} rather then n^k and p^k.

To discretize the partial derivative of the current density, Sharfetter and Gummel [14] made the hypothesis that on the segment from x_i to x_{i+1}, the values of J, D ($= \mu k_B T/q$) and E remain constant. This allows Eq. (2) to be integrated to obtain:

$$J = qDE\left(\frac{c_i}{1-\exp\left[\pm E(x_{i+1}-x_i)\right]} - \frac{c_{i+1}}{\exp\left[\pm E(x_i - x_{i+1})\right]-1}\right) . \tag{A.15}$$

By defining:

$$D = D_{i+1/2} \tag{A.16}$$

$$J = J_{i+1/2} \tag{A.17}$$

$$DB(i,\pm) = \frac{D_{i+1/2}}{h_i}\frac{\pm\Delta_i^k\psi}{e^{\pm\Delta_i^k\psi}-1} , \tag{A.18}$$

one obtains:

$$J_{i+1/2} = \pm q\left(DB_c(i,\pm)c_{i+1} - DB_c(i,\mp)c_i\right) . \tag{A.19}$$

The discretization thus gives:

$$\frac{\partial J_i}{\partial x} = \frac{J_{i+1/2}-J_{i-1/2}}{(h_i+h_{i-1})/2} . \tag{A.20}$$

The time discretization of:

$$\frac{\partial f}{\partial t} = H \tag{A.21}$$

is obtained by using:

$$\frac{f(t)-f(t-\Delta t)}{\Delta t} = sH(t) + (1-s)H(t-\Delta t) , \tag{A.22}$$

where s is a constant between zero and unity. The scheme $s = 1/2$ is a Crank–Nicolson-type implicit scheme, and $s = 1$ is a backward Euler. The discretized form leads to equations similar to Eq. (A.14). The density of trapped carriers can be readily computed using:

$$\begin{aligned} c_{t,i,j}^k = & \tfrac{\Delta t_j}{1+sk_r\Delta t_j}\left\{sk_c c_{i,j}^k + (1-s)k_c c_{i,j-1}^k \right. \\ & \left. + \left(\tfrac{1}{\Delta t_j} + (1-s)k_r\right)c_{t,i,j-1}^k\right\} . \end{aligned} \tag{A.23}$$

The criterion for the convergence of an iteration is:

$$\epsilon^k = \max\left\{\left|\tfrac{\psi_{i,j}^k-\psi_{i,j}^{k-1}}{\psi_{i,j}^k}\right|, \left|\tfrac{C_{i,j}^k-C_{i,j}^{k-1}}{C_{i,j}^k}\right|\right\} < \epsilon , \tag{A.24}$$

where ϵ is the relative precision wanted.

The x integral is computed using the formula [15]:

$$\int_{x_0}^{x_{N+1}} f(x)dx = h\left(\frac{109}{48}f_1 - \frac{5}{48}f_2 + \frac{63}{48}f_3 + \frac{49}{48}f_4 + \sum_{l=5}^{N-4} f_l + \frac{49}{48}f_{N-3} + \frac{63}{48}f_{N-2} - \frac{5}{48}f_{N-1} + \frac{109}{48}f_N\right) + O\left(\frac{1}{N^4}\right) , \quad \text{(A.25)}$$

while the time integral is simply obtained by:

$$\int_{t_1}^{t_M} f(t)dt = \sum_{j=1}^{M} f(t_j)dt(j) . \quad \text{(A.26)}$$

References

[1] A. Taroni and G. Zanarini, *Plasma effects and charge collection time in solid state detectors*, Nucl. Instrum. and Methods **67** (1969) 277.

[2] C.F. Williamson, J.-P. Boujot and J. Picard, *Tables of range and stopping power of chemical elements for charged particles of energy 0.05 to 500 MeV*, Rapport CEA–R 3042 (1966) 321.

[3] D.M. Caughey and R.E. Thomas, *Carrier mobilities in silicon empirically related to doping and field*, Proc. IEEE **55** (1967) 2192.

[4] S. Ramo, *Currents induced by electron motion*, Proc. I.R.E. **27** (1939) 584.

[5] H.K. Gummel, *A self-consistent iterative scheme for one-dimensional steady state transistor calculations*, IEEE Trans. Electron Devices **ED–11** (1964) 455.

[6] Application Software Group, CERN Program Library D506: *MINUIT Function Minimization and Error Analysis Reference Manual*, Version 92.1, i, (1992).

[7] F. Lemeilleur et al., *Electrical properties and charge collection efficiency for neutron-irradiated p-type and n-type silicon detectors*, Nucl. Phys. B, Proc. Suppl. **32** (1993) 415.

[8] Z. Li and H.W. Kraner, *Fast neutron radiation damage effects on high resistivity silicon junction detectors*, J. Electron. Mater. **21** (1992) 701.

[9] A. Chilingarov et al., *The electric field in irradiated silicon detectors*, ATLAS Note INDET–NO–194, 9 Dec. 1997.

[10] G. Casse et al., *Study of evolution of active volume in irradiated silicon detectors*, CERN–EP/98–61.

[11] C. Leroy et al., Proc. IVth Int. Conf. on Calorimetry in High Energy Physics, La Biola, Isola d'Elba, Italy, 19–25 Sept. 1993, eds. A. Menzione and A. Scribano (World Scientific, Singapore, 1994) p. 627.

[12] A. De Mari, *An accurate numerical steady-state one-dimensional solution of the p-n junction*, Solid-State Electron. **11** (1968) 33.

[13] G.A. Erskine, CERN Program Library F406: *Banded Linear Equations*, (1984).

[14] D.L. Scharfetter and H.K. Gummel, *Large-signal analysis of a silicon read diode oscillator*, IEEE Trans. Electron Devices **ED–16** (1969) 64.

[15] W.H. Press, B.P. Flannery, S.A. Teukolsky and W.T. Vetterling, *Numerical Recipes in C*, Cambridge University Press (1991) p. 123.